Investigation on the Effect of Thrust Chamber Geometric Parameters on the Performance of NTO/MMH Thrusters

P. Arun Kumar, C. Rajeev Senan, B. Ajith, M. Ponnuswamy, P. Balachandran

Abstract: Hypergolic bipropellant radiation cooled thrusters utilizing Mono-methyl Hydrazine and Nitrogen Tetroxide are commonly used in spacecraft missions for attitude and orbit control. The performance index of a rocket engine is the specific impulse which is a function of combustion efficiency, known as C* efficiency, and the nozzle efficiency. An experimental investigation is carried out to evaluate the effect of combustion chamber design parameters on performance(C*efficiency) for varied injector spray and atomisation characteristics as well as injection pressures. Analytical model with empirical correlation available in the literature is used as a tool for understanding the physical process in the combustion chamber and predicting C* efficiency which was validated with experiments. Design variables considered are characteristic length and the contraction ratio. Cold flow evaluation of the injector using simulant water was done to evaluate the droplet size and injection velocity, which is normalised to the propellant flow conditions. Hot test for 10s using the stainless steel chamber was done at sea level with instrumentation for chamber pressure, mass flow rate of propellants and throat temperature. Results show that for a given injection and operating conditions, there exists a range of L* and contraction ratio where C*efficiency will be optimum and less sensitive. Trends in throat temperature measured are also evaluated. This paper presents the details of the investigation.

Keywords: Hypergolic bipropellants, C* efficiency, L*, Contraction Ratio

I. INTRODUCTION

Small rocket engines are typically employed in propulsion applications requiring relatively low thrust levels and total impulse. Thrusters using hypergolic bipropellants consisting of NTO and MMH provide the greatest benefit of the ability to initiate multiple starts which is of primary importance for pulsing applications. The thrust chamber is the combustion device where the liquid propellants are injected, vaporized, mixed and burned to form hot gaseous reaction products, which in turn are accelerated and ejected at high velocity.

Dr. P. Arun Kumar*, Group Head, Spacecraft Propulsion Engines Group (SPEG), Liquid Propulsion Systems Centre, Valiamala P.O, Trivandrum-69554, Kerala, India.

C. Rajeev Senan, Engineer-SF, Spacecraft Propulsion Engines Group (SPEG), Liquid Propulsion Systems Centre, Valiamala P.O, Trivandrum-69554, Kerala, India.

B. Ajith, Engineer-SE, Spacecraft Propulsion Engines Group (SPEG), Liquid Propulsion Systems Centre, Valiamala P.O, Trivandrum-69554, Kerala, India.

M. Ponnuswamy, Engineer-SE, Spacecraft Propulsion Engines Group (SPEG), Liquid Propulsion Systems Centre, Valiamala P.O, Trivandrum-69554, Kerala, India.

Dr. P. Balachandran, Principal, Pinnacle School of Engineering and Technology, Areeplachy P.O, Anchal, Kollam-691333, Kerala, India.

For the thrust chamber design, the starting point is to finalize the combustion chamber geometry followed by nozzle design. Even though the basic atomization is described in many of the literature, the combustion mechanism of hypergolic propellants is different from non-hypergolic of which few published literatures are available. The total combustion process, from injection of reactants until completion of the chemical reactions and conversion of the products into hot gases, requires finite amount of time and volume, as expressed by the characteristic length, L*

$$L^* = \frac{V_c}{A_{thr}} = \frac{m_{pt}v_s t_s}{A_{thr}} \quad (1)$$

This factor is significantly greater than the linear length between injector face and the throat plane. Typically, large scale engines are constructed with a low contraction ratio and a comparatively long length, and smaller thrust chambers employ a large contraction ratio with a shorter length, while still providing sufficient L* for adequate vaporization and combustion dwell time. In general, combustion process is not scalable and optimum combustion chamber geometry is arrived at by experimentally evaluating the performance by changing L* and contraction ratio. In the early 60s, a widely accepted attempt was undertaken by Priem and Heidmann[1,2] suggesting propellant vaporization as design criterion for rocket engine combustion chambers. Though limited to a simplified, one-dimensional description of reactive flows in liquid or gas bi-propellant rocket motors, their model could show and explain fundamental effects of propellant properties, spray conditions, chamber geometry and operating parameters on combustor performance and efficiency whenever propellant vaporization could be considered as the rate-controlling step. In the present investigation, this model is used to predict the performance namely C* efficiency for the given thrust chamber geometry and operating conditions validated with hot tests. A common injector is used for all the tests and for each thrust chamber geometry, identical operation conditions are ensured by maintaining propellant flow Reynolds number and Weber number within a narrow band.

II. ANALYTICAL MODEL

2.1. Selection of Model

From a physical point of view, the mechanism occurring within the combustion chamber of a storable bipropellant rocket engine are manifold and fairly complex. A reactive gaseous phase (first phase), two dispersed droplet phases(second phase) and eventually a liquid cooling film(third phase) exist simultaneously and interact with each other.

Hypergolic ignition is somewhat different due to the exothermic liquid/vapour chemical reactions which initiate combustion throughout the combustion chamber, rather than from a localized point. The dominant ignition reactions of these hypergols when injected as liquids have been found to be gas phase as the pre-ignition reactions for a propellant combination like NTO/MMH have been shown to start in a gas phase[3,4,5]. Gas phase reaction contributes a large share of the total heat release. Reasonable predictions of the combustion flow field depend on the fully understanding of physical-chemical phenomena and the exact analytical descriptions. Many aspects of hypergolic propellant combustion have been studied in the past but much remains to be done, especially in utilizing the recent developments in chemical kinetics within a computational fluid dynamics framework. Some of the complex interactions of fundamental processes have been probed theoretically using various empirical parameters, but there remains a need for a comprehensive model which encompasses the phenomena involved in hypergolic ignition and combustion. Few studies[6,7] reported were aimed at such an inclusion of chemical kinetic aspects of hypergolic propellant combustion into fluid dynamic calculations to understand the nuances of the interactions involved. It is reported[8] that in the combustion of NTO/MMH combination, 403 elementary reactions and 81 species are involved. It is emphasized that only little information can be found in open literature on chemical kinetic aspects. Moreover, it may be noted that chemical reaction rates are not rate limiting in thrust chamber combustion process involving storable hypergolic propellants at nominal/design mixture ratio due to low reaction time which is of few milliseconds and only at extreme/non nominal mixture ratio situations this will be significant. According to a study by B.P.Green et al[9] hypergolic combustion remains primarily evaporation controlled as long as reasonable good premixed conditions are generated by an injector. Therefore it is postulated that the atomization/vaporization process is usually the rate-limiting combustion for these combinations in the nominal mode of mixture ratio. It is also reported[10] that the contribution of atomization/vaporization is significant(0-8%) in the energy release loss in comparison with chemical reaction loss(<1%).   Model developed by Priem gives a qualitative trend for variations in thrust chamber geometry, atomization and operating conditions on the performance which is of interest in this experimental investigation. However for quantitative evaluation of performance, like in any other analytical models, accurate information on atomization characteristics is required through validation tests.   Also this model can be applied to following situations: Vaporisation of one of the propellant is controlling the reaction while the other is already completely vaporised.Droplet shattering does not take place (Weber number of propellant evaluated is < 10). Below critical point conditions prevail in the combustion chamber.

As the current study meets the requirements listed above, this model has been considered for the investigation.

2.2. Model Description

In the analytical model developed by Richard J. Priem and Marcus F. Heidmann, calculations of the vaporization rate and history show the effects of propellants, spray conditions, engine design parameters, and operating parameters on the vaporization process.   The equations needed for the calculations are based on the assumption that vaporization process is the rate controlling step.   The effective combustion chamber length L_{ef} required to vaporize 90 percent of the total mass of individual propellant spray is given by:

$$L_{ef} = \left(\frac{L_c}{CR^{0.44}} + \frac{0.83L_N}{CR^{0.22}S^{0.33}}\right) * \frac{(\frac{P_c}{300})^{0.66}}{(1 - T_{I.O.R})^{0.4}(\frac{r_m}{0.003})^{1.45}(\frac{u_o}{1200})^{0.75}} \quad (2)$$

The effective utilization factor, $L_{eff\ util}$ of the combustion chamber expressed in percentage for the propellant considered is defined as the ratio of L_{ef} / L_c is computed. The MR_v is then calculated using the relation:

$$MR_v = MR_m \left(\frac{L_{eff\ util(O)}}{L_{eff\ util(F)}}\right) \quad (3)$$

(4)

$C^*_{eff(pred)}$ is computed from C^*_{th}[11] using the relation:

$$C^*_{eff(pred)} = (C^*_{th(v)} \dot{m}_{pv}) / (C^*_{th(t)} \dot{m}_{pt})$$

III.   TEST ARTICLE

Injector is a coaxial swirl single element made of titanium alloy, Ti6Al4V. In a swirl injector, the liquid is fed into the swirl chamber through tangential inlet channel. At the injector nozzle exit, the jet will be converted into a conical film which is further broken into drops. The inherent characteristics of the injector aid in an unintentional film cooling of the thrust chamber. Two types of injectors having identical flow rates but different flow patterns are evaluated. Mark1 with fuel flow through outer passage forming a onion pattern as shown in figure-1 and mark2 with fuel through inner passage and forming a conical diverging flow pattern as shown in figure-2 were evaluated so that MMD_Fmark1>MMD_Fmark2 and injection velocity of fuel, u_{oF}mark1<u_{oF}mark2. Corresponding Re no. and We no. of mark2 injector is also greater than that of mark1. Since fuel vaporization is the rate controlling process in this study, focus is on the spray and atomisation characteristics of fuel spray rather than on the oxidizer. This aspect is further explained in the subsequent section. Figures-1 & 2 show the fuel spray pattern using demineralised water as simulant fluid.

Contraction ratio, CR of a thrust chamber is the ratio of the cross sectional area of the combustion chamber to the cross sectional area at the throat. In this investigation, the cross sectional area at the throat is not changed. Three types of thrust chambers made up of stainless steel (SS304) with different contraction ratio(type1:CR-12.42, type2:CR-16.96 and type3:CR-28.03) but having the same convergent angle of 28Degree were realised.

CR was varied by changing the inner diameter of the combustion chamber. For type2 thrust chamber, additional 10Degree convergent angle hardware was also realised.
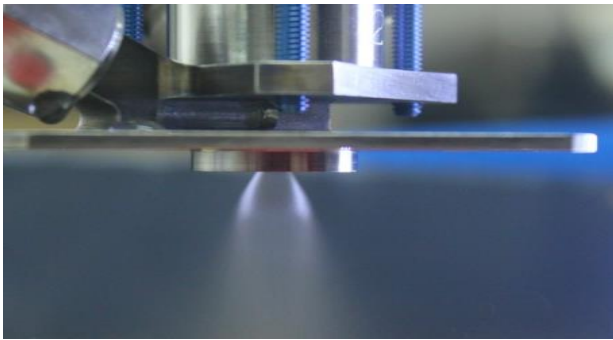

Figure-1 Fuel Spray Pattern of Mark1

Figure-2 Fuel spray pattern of Mark2

The injector assembly is connected to the thrust chamber by a screw joint. L* is varied by using spacers of thickness 2×10^{-3}m, 5.1×10^{-3}m, 11.6×10^{-3}m and a combination of it assembled in-between the chamber and the injector as shown in figure-3. Because of this, the range of L* achieved is given in the table-1.

Table-1 L* variation table

Type	Contraction ratio (CR)	L*
1	12.47	0.62m - 0.91m
2	16.96	0.598m – 1.01m (For convergent angle of 10Degree :0.622m – 1.032m)
3	28.03	0.62m – 1.31m

Figure-3 Thruster assembly with Mark1 and type1 (with 11.16×10^{-3}m thick spacer) chamber

Solenoid operated flow control valves are used for on/off operations. Figures-4 shows the cross section of thrust chamber.
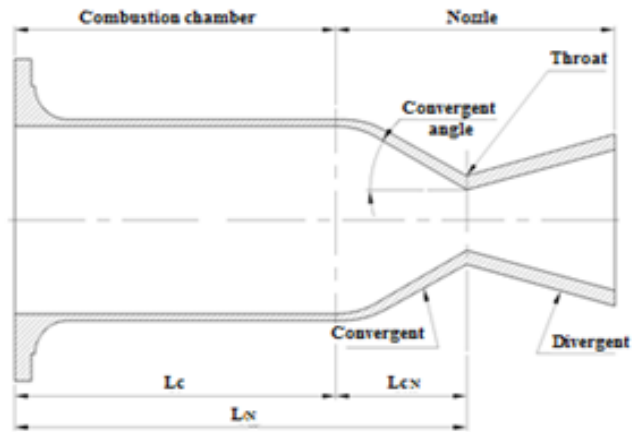

Figure-4 Cross section of Thrust Chamber

IV.   TESTING- COLD AND HOT
4.1. Cold flow Evaluation

This test using demineralized water as simulant at different injector pressure drops(ΔP) is done to evaluate the injection velocity, u_o and MMD. ΔP considered corresponds to HIP, MIP and LIP operating conditions. Visual characteristics of the sprays are determined by studying the images obtained by high resolution digital camera for the individual inner and outer flow patterns. From this, flow cone angle 2α at the injector nozzle exit and MMD are obtained. Difference in flow cone angle for water and propellant is assumed to be negligible[12]. Using 2α measured as the value for individual propellants, the following equations [13] are used to determine the co-efficient of discharge, C_d by iterative method.

$$tan\alpha = \frac{2C_d A_s}{\sqrt{\left[1+\sqrt{(1-\phi)}\right]^2 - 4C_d^2 A_s^2}} \quad (5)$$

$$C_d = \frac{1}{\sqrt{A_s^2 \Big/ \left\{(1-\phi) + \frac{1}{\phi^2}\right\}}} \quad (6)$$

The swirl number, As is given by:

$$A_s = \frac{(1-\phi)\sqrt{2}}{\sqrt{\phi^3}} \quad (7)$$

Injection velocity, u_o is derived from the relation:

$$u_o = \frac{\dot{m}_p}{\rho_p C_d A} \quad (8)$$

Reynolds number, Re and Weber number, We are defined as[14]:

$$R_e = \frac{\rho_p u_o L_{ch}}{\mu_p} \qquad (9)$$

$$W_e = \frac{\rho_g u_o^2 L_{ch}}{\sigma_p} \qquad (10)$$

While the characteristic length, L_{ch} for the inner spray is set equal to the inner diameter, d_i of the inner orifice and for the outer spray, it is the difference of inner diameter of the outer orifice to the outer diameter of inner diameter, $d_o - d_{in}$ as illustrated in the following figure-5.
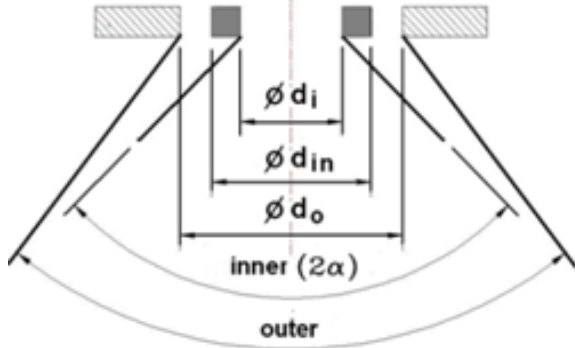

Figure-5 Schematic of the swirl injector

MMD measured using water is converted to propellant condition using the relation[3].

$$MMD_P = MMD_w \left(\frac{\rho_w \sigma_p \mu_p}{\rho_p \sigma_w \mu_w} \right)^{1/4} \qquad (11)$$

Results of cold flow evaluation normalised to propellant flow are given in the following tables-2 and 3.

Table-2 Cold flow evaluation summary of Mark1

Pattern	Condition	Spray cone angle, 2α	Injection velocity u_o, m/s	MMD_p, microns
Inner (Oxidiser)	HIP	68.0	17.24	37.37
	MIP	66.4	16.97	45.93
	LIP	63.1	16.67	48.66
Outer (fuel)	HIP	100.0	14.92	114.28
	MIP	96.7	14.56	124.17
	LIP	79.9	13.39	136.00

Table-3 Cold flow evaluation summary of Mark2

Pattern	Condition	Spray cone angle, 2α	Injection velocity u_o, m/s	MMD_p, microns
Inner (fuel)	HIP	68.2	21.53	76.55
	MIP	66.6	21.12	88.45
	LIP	63.5	20.62	102.9
Outer (oxidiser)	HIP	107.8	14.01	35.42
	MIP	104.0	12.19	38.92
	LIP	100.0	11.75	54.49

It may be noted that the injection velocity of the inner flow is always higher than outer flow due to the geometric characteristics of swirl injector.

4.2. Hot Testing

Hot burn using the stainless steel(SS304) combustion chamber was done at sea level(10s) for each condition with instrumentation for chamber pressure(accuracy of ±0.5%), mass flow rate(accuracy of ±0.3%), of propellants and throat temperature(accuracy of ±1.0%). Temperature which is maximum at the throat in a radiation cooled thrust chamber is measured using thermocouple welded at the outer surface of throat. Injectors which were subjected to the cold flow evaluation were used in all hot tests with a flanged joint thrust chamber and separate series of tests were conducted using mark1 and mark2 injectors. Same thrust chamber was tested with mark1 as well as mark2 injector. Combustion chamber length was varied using spacers with thickness in steps of 0(no spacer), 2, 5.1, 7.1, 11.6, 16.7 & 23.2×10^{-3}m for each type of CR(Type1-CR:12.47, Type2-CR:16.96, Type3-CR: 28.03). This has resulted in an L* variation of 0.62 to 0.91m for type1, 0.598 to 1.01m for type2 and 0.62 to 1.31m for type3 respectively. Totally one hundred and twenty six hot tests (2 injector's, 3 CR's, 7 steps of L* and 3 injection pressure conditions) were carried out. Additionally convergent angle was varied in one CR(16.96) thrust chamber to evaluate its effect on the performance resulting in another 42 tests(2 injector's, 1CR, 7 steps of L* and 3 injection pressure conditions).

Figure-6 Thruster undergoing sea-level firing

168 hot tests were carried out as part of the study. In the entire test series, mixture ratio was maintained within 1.64 ±0.07 at HIP whereas at MIP and LIP, there were minor deviations and the above figure-6 shows a hot test.

Performance parameter C* efficiency which is a measure of combustion efficiency is computed using the following equation.

$$C^*_{eff(exp)} = \frac{P_c * A_{thr} * 100}{\dot{m}_{pt} * C^*_{th}} \qquad (12)$$

For simulating identical condition for comparison, the injector flow Reynolds number and Weber number are maintained within a narrow band for each version(mark1 & mark2) test series at a particular injection pressure condition as shown in figures-7 and 8 below at HIP condition and it is similar at MIP and LIP conditions.
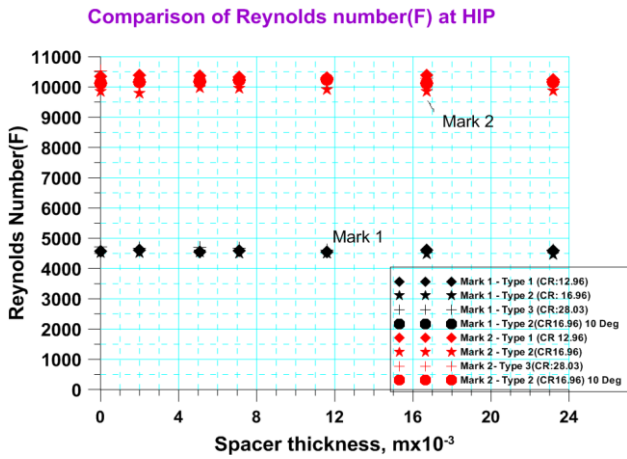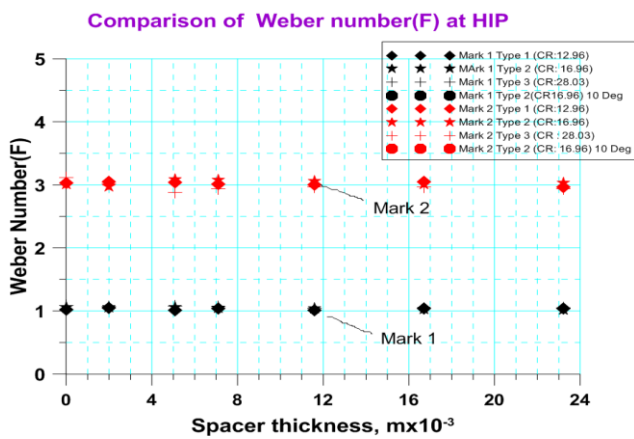
Figure-7 Mark1 & Mark2 Reynolds No. (Fuel) Plot at HIP

Figure-8 Mark1 & Mark2 We No.(Fuel) at HIP

V. METHODOLOGY OF EVALUATION

Experiment value of C* efficiency($C^*_{eff(exp)}$) is derived from the measured hot test parameters as explained previously. Complete vaporization of oxidizer(NTO) takes place due to the lower critical temperature as well as smaller droplet size of NTO compared to that of MMH and hence vaporization of fuel(MMH) is considered as the rate controlling process of combustion in this investigation.

Initially C^*_{eff} was predicted(pred) from $L_{eff\ util}$ by assuming the actual combustion chamber length as L_{c90} and L_{ef} was computed from the empirical correlation in the analytical model. Comparison of $C^*_{eff(exp)}$ with $C^*_{eff(pred)}$ indicates disparity exceeding ±5% expected for this method of analysis for the first version injector(mark1) whereas it is within the limit for the second version(mark2). This is due to the error in MMD value taken for the decisive propellant which is MMH for this study as the fuel spray formation is in the onion stage for the mark1 injector as against the conical diverging pattern in mark2.

Since there is an uncertainty in the assumption that L_{c90} is same as the combustion chamber length in the computation of $L_{eff\ util}$, another method of approach is attempted by calculating $L_{eff\ util}$ from the experimental value of C* efficiency in one test series considered as a reference/model test series. In this method, L* variation test series using mark1 injector and type2 thrust chamber with CR of 16.96 and convergent angle of 28Degree is taken as the reference/model test series.

Experimentally derived value of $L_{eff\ util}$ from the reference/model test series is used to predict the C* efficiency for the L* variation test series on the remaining thrust chamber geometry using mark1 injector as well as for all the types of thrust chamber geometry using mark2 injector. Disparity between prediction and experiment value of C* efficiency is within the limit by this approach except for mark2 with type1 at LIP in the test series as shown in the following tables-4 and 5.

Table-4 Mark1 comparison of C* efficiency after validation correction on MMD (fuel)

Type	Injection pressure	Average $C^*_{eff(pred)}$, %	Average $C^*_{eff(exp)}$, %
1 (CR 12.47)	HIP	91.40	92.06
	MIP	91.73	91.54
	LIP	85.86	92.40
2 (CR 16.96)	HIP	96.31	94.39
	MIP	96.63	94.03
	LIP	91.20	94.94
2 (CR 16.96) 10^{0}Conv. angle	HIP	97.74	94.08
	MIP	98.75	94.11
	LIP	93.12	94.36
3 (CR 28.03)	HIP	98.10	94.46
	MIP	98.02	94.54
	LIP	96.09	95.12

Table-5 Mark2 comparison of C* efficiency after validation correction on MMD (fuel)

Type	Injection pressure	Average $C^*_{eff(pred)}$, %	Average $C^*_{eff(exp)}$, %
1 (CR 12.47)	HIP	96.66	90.47
	MIP	84.87	91.91
	LIP	78.37	92.00
2 (CR 16.96)	HIP	99.24	96.1
	MIP	96.66	92.06
	LIP	83.05	92.1
2 (CR 16.96) 10^{0}Conv. angle	HIP	100	94.58
	MIP	100	92.78
	LIP	97.9	91.48
3 (CR 28.03)	HIP	99.34	90.16
	MIP	94.27	90.80
	LIP	88.82	89.26

Following figures-9 to 11 give the details for the model test series at three pressure conditions for the injector-thrust chamber combination of mark1 and type2. $L_{eff\ util(F)}$ is the experiment value deduced from $C^*_{eff(exp)}$ as explained previously.
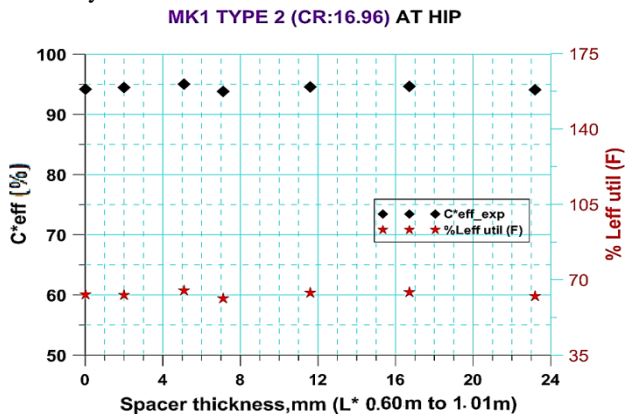

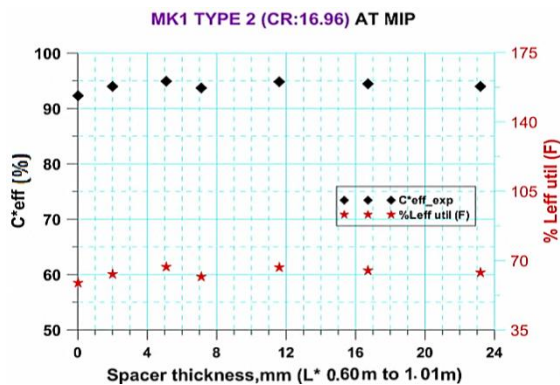**Figure-9 Mark1 with type2 at HIP- L* on performance**

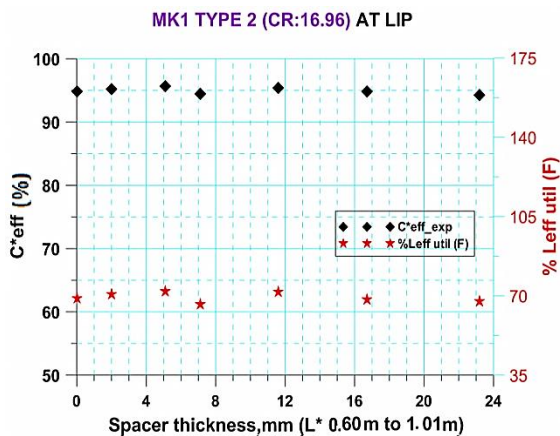**Figure-10 Mark1 with type2 at MIP- L* on performance**

Figure-11 Mark1 with type2 at LIP- L* on performance

VI.   RESULTS AND DISCUSSION

Analysis is done to assess the effect of the design variables (L*,CR and convergent angle) on performance at the three injection pressures evaluated in this study. Following are the findings of the investigation.

6.1. Effect of L*

In this section, evaluation is done to assess the effect of variation in L* on C^*_{eff} and throat temperature for the two version injectors. Three types of thrust chambers evaluated

are having the same convergent angle of 28Degree. L* is varied by using spacers with identical thickness in each type of thrust chambers. It may be noted that the same type of thrust chamber is used in the hot test evaluation with the two version injectors. $L_{eff\ util(F)exp}$ refers to experiment values deduced from $C^*_{eff(exp)}$ for the test series evaluated. Predictions for the test series are made using $L_{eff\ util(F)exp}$ of model test series assuming it to be the same for other test series as mentioned previously. It may be noted that since full vaporization of oxidizer takes place for all the cases in this investigation, trends in $C^*_{eff(pred)}$ and $L_{eff\ util(F)pred}$ are identical to the model test series as utilization factor is not changed.

Observations on performance variation with L* are summarized below.

Difference between $C^*_{eff(pred)}$ using the model and $C^*_{eff(exp)}$ is within the permissible range of ±5 %. However trend of predictions depend on reference/model test series as shown in the following figures-12 and 13.

Two regimes of L* namely lower(L*<0.68m) and higher(L*≥0.68m) are identified where the sensitivity of performance($C^*_{eff(exp)}$) and throat temperature are different as indicated in figures-12 to 14 for type3 case. Zero spacer point corresponds to lower regime for this case.
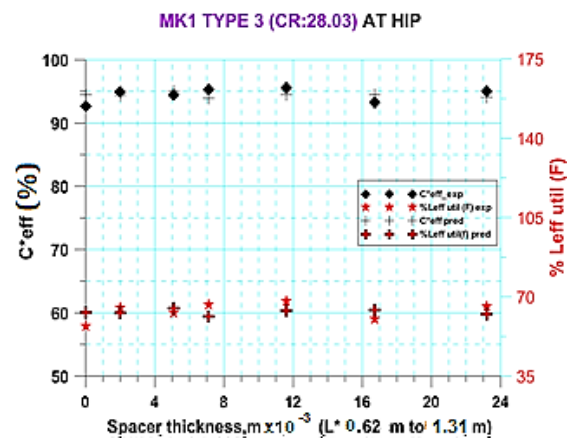

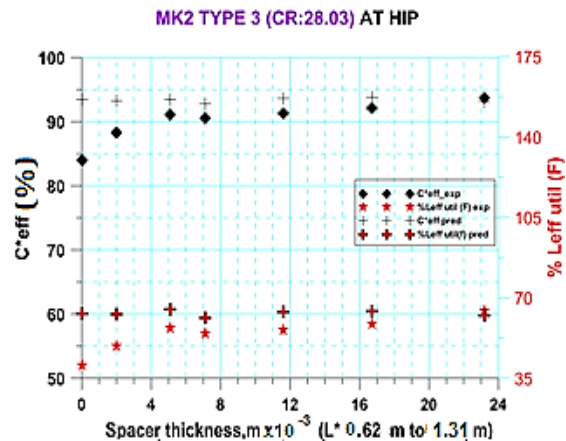**Figure-12 Mark1 with type3 at HIP- L* on performance**

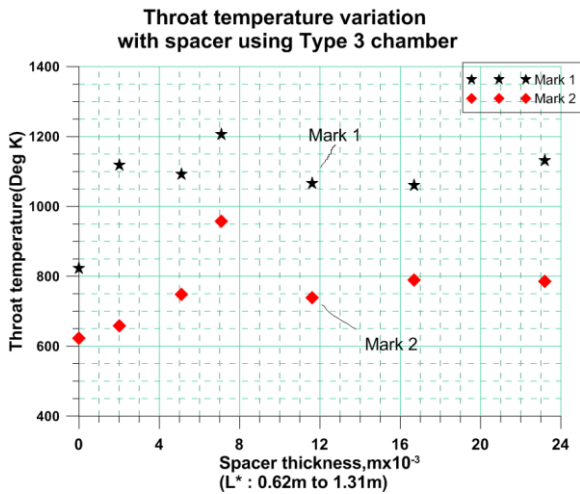
Figure-13 Mark2 with type3 at HIP- L* on performance

Figure-14 Mark1& Mark2 with type3 at HIP-L* on throat temperature

In higher L* regime, variations in $C_{eff(exp)}$ is marginal and within the measurement accuracy of ±1%. Throat temperature is also less sensitive to change in chamber length and variations are random in nature.

In lower L* regimes as shown in above plots, $C^*_{eff(exp)}$ is sensitive to chamber length. This due to the fact that L_N the distance of the throat from the fuel injection point is very low for this regime. Type3 with maximum CR is having the largest combustion chamber inner diameter resulting in lowest L_N of 35.01×10^{-3}m in comparison with other two types(type1:58.37×10^{-3}m and type2:43.92×10^{-3}m) in identical case of no spacer. This reduces the stay time t_s of the propellant in the chamber till it reaches throat as vaporization and combustion reaction takes place upto the throat.

With increase in spacer thickness, L_N increases which in turn improves t_s and hence $C^*_{eff(exp)}$ increases. Similar observations are reported by investigators[7,15,16,17] for engines using hypergolic propellants. Abovementioned observation in $C^*_{eff(exp)}$ is not seen in $C^*_{eff(pred)}$ as the reference/model test series of type2 has not captured this trend due to its higher L_N even though the disparity between experiment and prediction of C^*_{eff} is within the acceptable limit for this case. Influence of L_N indicates that vaporisation is a dominant rate controlling process in combustion of hypergolic propellant as it affects the stay time. Throat temperature is also sensitive in this regime.

Due to the difference in spray characteristics, throat temperature in mark2 injector test series is relatively lower as the dry out point of film cooling is near to the throat in comparison with mark1 injector test series. Though performance plots shown are at HIP, trends are identical at MIP and LIP.

6.2. Effect of CR

CR variation study shows that thrust chamber geometry influences differently on performance at each injection pressure condition as well as regimes of L* depending on spray characteristics as explained below.

Individually for mark1 & mark2 test series, comparison is done at an approximately fixed L* value of 0.68m for each CR. For type1 and type2 thrust chambers, near L* value of 0.68m is achieved using spacer thickness of 5.1×10^{-3}m(third data point in the test series) and in type3 with spacer

thickness of 2×10^{-3}m(second data point). In the lower L* regime, no spacer case is considered for assessment. Trends are different for higher(L*≥0.68m) and lower(L*<0.68m) regime cases of thrust chambers in mark1 and mark2 test series.

Table-6 Mark1 Performance summary for lower L*(less than 0.68m)

Condn	TYPE	L* m	$L_N \times 10^{-3}$m	$C^*_{eff(pred)}$ %	$C^*_{eff(exp)}$ %	Throat temp K
HIP	1	0.621	58.37	94.28	91.66	940
	2	0.598	43.92	------	94.22	962
	3	0.622	35.01	94.47	92.68	823
MIP	1	0.621	58.37	92.80	90.82	901
	2	0.598	43.92	-------	92.34	911
	3	0.622	35.01	92.70	92.29	770
LIP	1	0.621	58.37	94.73	93.17	841
	2	0.598	43.92	-------	94.83	835
	3	0.622	35.01	94.98	91.17	759

Table-7 Mark2 Performance summary for lower L*(less than 0.68m)

Condn	TYPE	L* m	$L_N \times 10^{-3}$ m	$C^*_{eff(pred)}$ %	$C^*_{eff(exp)}$ %	Throat temp K
HIP	1	0.621	58.37	93.75	89.55	766
	2	0.598	43.92	93.15	95.62	925
	3	0.622	35.01	93.42	84.03	623
MIP	1	0.621	58.37	92.25	91.50	821
	2	0.598	43.92	91.72	91.45	831
	3	0.622	35.01	91.91	83.15	652
LIP	1	0.621	58.37	94.68	89.77	868
	2	0.598	43.92	94.30	91.33	774
	3	0.622	35.01	93.98	84.48	615

For L*<0.68m, referring table-6, in mark1, $C^*_{eff(exp)}$ shows a marginal variation except at LIP where there is a decrease in value of more than±1% from type2 to type3. As mentioned earlier, type3 chamber with no spacer(L* of 0.622m) is having the shortest L_N of 35.01×10^{-3}m among the hardwares realised. Also at LIP, MMD of fuel will be coarser as shown in table-2. Referring equation 3, this coarser MMD of fuel will result in lower $L_{ef(F)}$ which in turn decreases $L_{eff\ util(F)}$ and it can result in insufficient stay time for the fuel droplet vaporization.

This will lower the $C^*_{eff(exp)}$. However as already discussed before, prediction could not capture this trend as it is not seen in the model test thrust chamber(type2) which is having a better design in terms of L_N for the spray characteristics in comparison with type3.

Lower values of L_N improves the effective film cooling at the throat as it is near to the fuel injection point lowering the throat temperature which is also explained previously.

Above observations show that in lower L^* regimes, L_N will be influencing the performance and throat temperature when injection pressure is decreased beyond a threshold value. These findings are in line with the previous investigation[18] on a small thruster.

Table-7 shows that, in mark2, at HIP alone, there is a notable increase in $C^*_{eff(exp)}$ from type1 to type2. At all the injection pressure conditions, $C^*_{eff(exp)}$ is maximum at type2 and there is an appreciable reduction from type2 to type3. Decrease in $C^*_{eff(exp)}$ from type2 to type3 at all injection pressure conditions is due to L_N, which is lowest for type3 with no spacer case.

Throat temperature in mark2 injector test series is relatively lower in comparison with mark1 injector test series due to the difference in spray characteristics mentioned earlier.

For $L^* \geq 0.68m$ regime, referring figures-15 & 16, irrespective of fuel injection spray characteristics of the injector evaluated(mark1 version or mark2 version injector), $C^*_{eff(exp)}$ peaks around type2 even though L_N decreases from $58.37 \times 10^{-3}m$ to $43.92 \times 10^{-3}m$ initially with increase in CR.

Above said observation is true at MIP as well as LIP conditions. This shows the influence of CR on $C^*_{eff(exp)}$ in higher L^* regimes. Throat temperature trend also follows $C^*_{eff(exp)}$ trend as seen in figure-17.
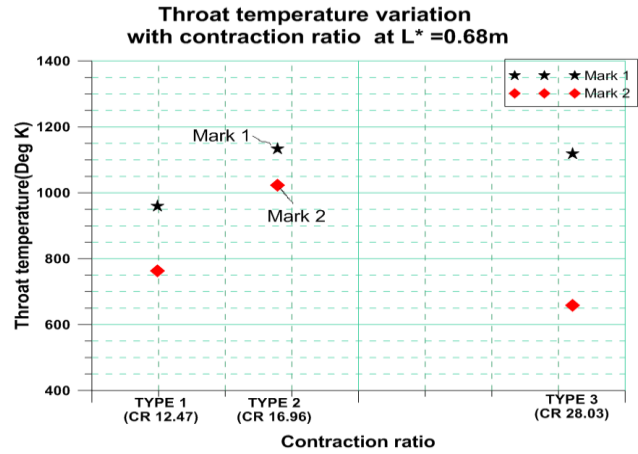

Figure-15 Mark1 Effect of CR on Performance at HIP

Figure-16 Mark2 Effect of CR on Performance at HIP

Figure-17 Mark1 & Mark2 Effect of CR on Throat Temperature at HIP

6.3. Effect of CR Angle

Referring figures-18 & 19, irrespective of fuel injection spray characteristics of the injector evaluated(mark1 version or mark2 version injector): Sensitivity of $C^*_{eff(exp)}$ for convergent angle variation from 28Degree to 10Degree is less and random in nature as variation is marginal and within the measurement accuracy of ±1%. Throat temperature for 28Degree convergent angle thrust chamber is higher than 10Degree convergent angle thrust chamber as observed in figures-20 & 21. It is reported[19] that with lower throat inner diameter and higher convergent angle, convective heat transfer coefficient can be higher at the throat. In this study, 28Degree convergent angle thrust chamber realised is having lower throat inner diameter of $3.352 \times 10^{-3}m$ against 10Degree convergent angle thrust chamber throat inner diameter of $3.395 \times 10^{-3}m$. This could be the reason for the higher temperature observed in 28Degree convergent angle thrust chamber though $C^*_{eff(exp)}$ values are comparable in both the thrust chambers.

Due to the difference in spray and atomisation characteristics, throat temperature in mark2 injector test series is relatively lower in comparison with mark1 injector test series.
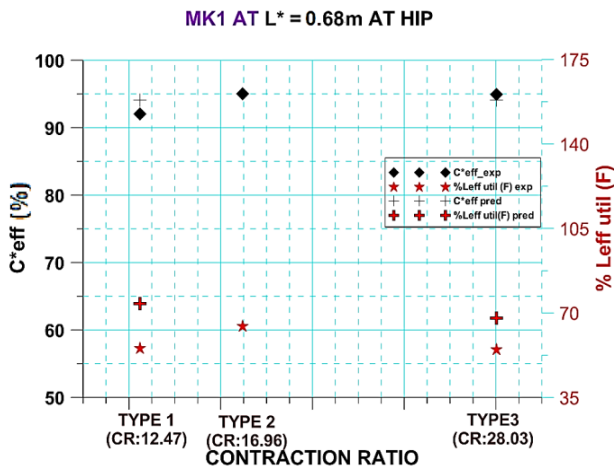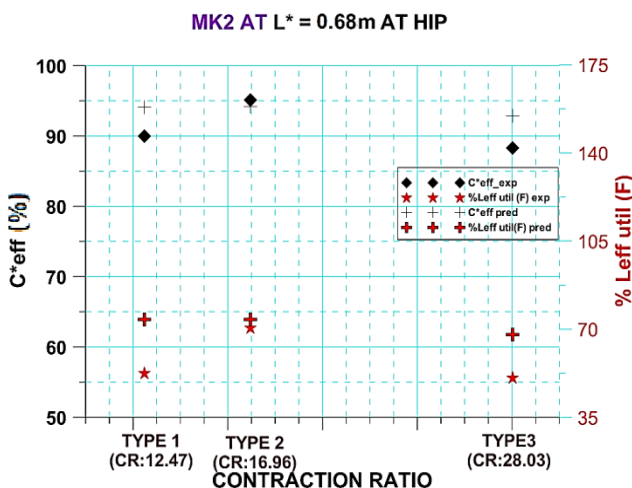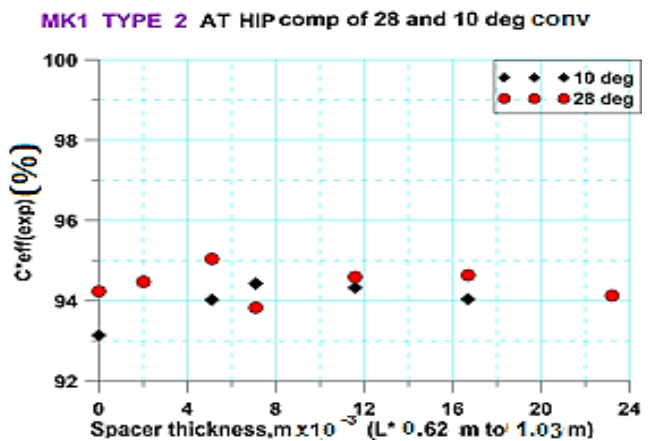

Figure-18 Mark1 with type-2 and with 28 & 10 Degree Convergent angle at HIP-L* on performance
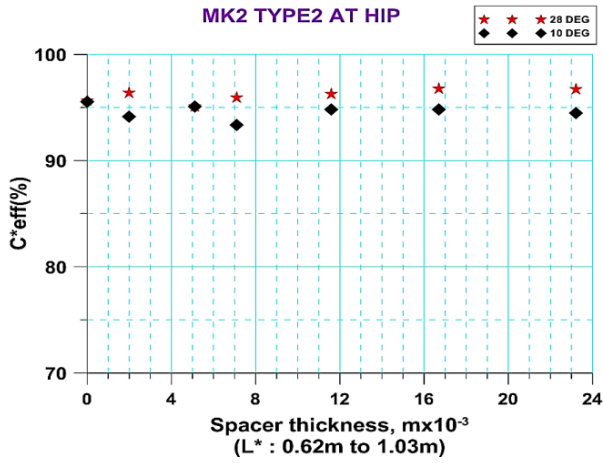
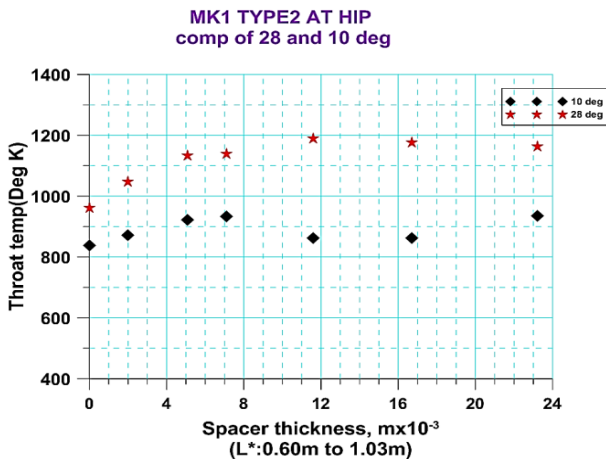**Figure-19 Mark2 with type-2 and with 28 & 10 Degree convergent angle at HIP-L* on performance**

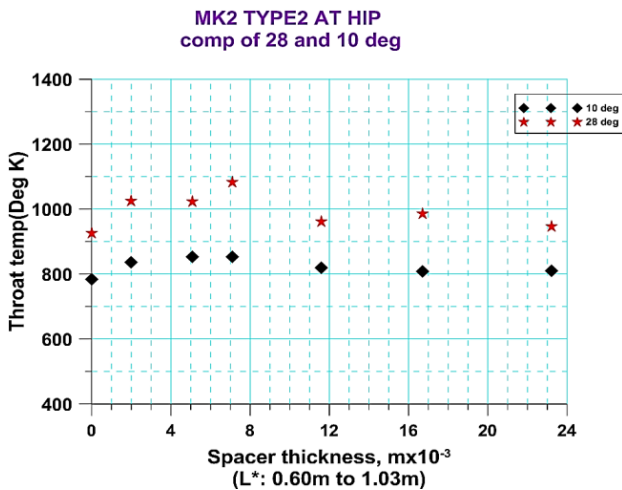**Figure-20 Mark1 with type2 and with 28 & 10Degree convergent angle at HIP -L* on throat temp.**

Figure-21Mark2 with type2 and with 28 & 10Degreeconvergent angle at HIP- L* on throat temp.

Abovementioned observations are same at MIP & LIP conditions.

6.4. Effect of Injection Pressure

To have a better understanding on the effect of injection pressure on performance, comparison of performance is done for a fixed spacer and L* for each CR. Details of a typical case for 7.1×10^{-3}m thick spacer which represents the middle point of a test series is given below for mark1 & mark2. Though this case belongs to higher L*(L*≥0.68m)

regime, observations are identical in lower L* and higher L* regimes. Thrust chambers with 28Degree convergent angle alone is considered for analysis.
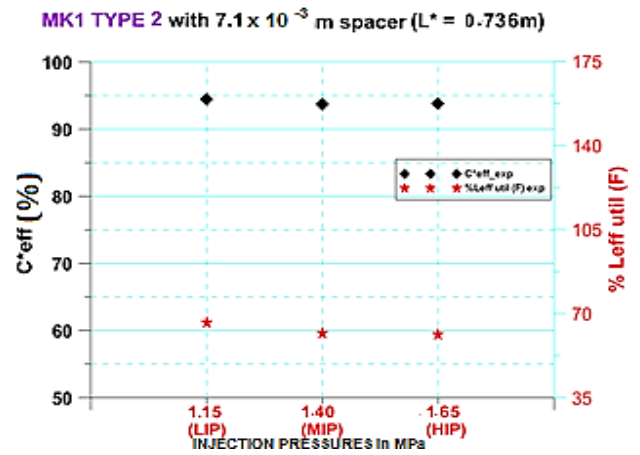

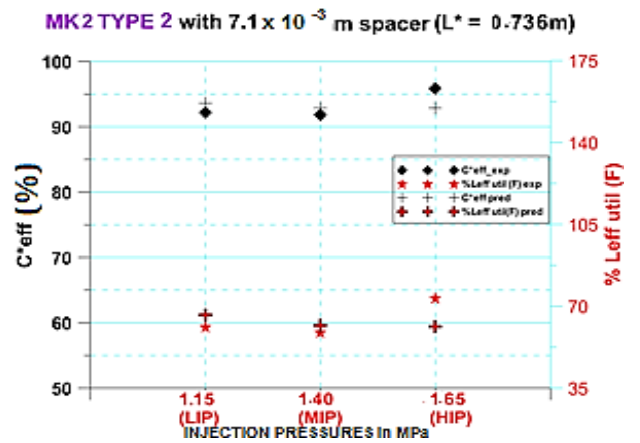**Figure-22 Mark1 with type2 at 7.1×10^{-3}m spacer - Injection pressure on performance**

Figure-23 Mark2 with type2 at 7.1×10^{-3}m spacer - Injection pressure on performance

Referring figure-22, sensitivity of $C^*_{eff(exp)}$ with injection pressure is marginal in mark1. In mark2 test series as shown in figure-23, type2 thrust chamber alone indicates over 4% reduction in $C^*_{eff(exp)}$ from HIP to MIP in the test series. It may be noted that in type2 with mark2 injector, $L_{eff\ util(F)exp}$ is maximum(73.29%) at HIP with a $C^*_{eff(exp)}$ value of 95.91% as against the corresponding values of 61.31%($L_{eff\ util(F)exp}$ and 93.80%($C^*_{eff(exp)}$) when used with mark1 at the same HIP. In mark1 and type2 combination, maximum values of $L_{eff\ util(F)exp}$ and $C^*_{eff(exp)}$ are observed at MIP. Abovementioned observations show different trends when the same type of thrust chamber is tested with two injectors having different spray and atomization characteristics. This indicates that each thrust chamber geometry will be optimum at different injection pressure for a specific spray and atomization characteristics. Though the difference between experiment and prediction values of $C^*_{eff(exp)}$ are within the acceptable limits in mark2 series also, trend of predictions depends on model test series.

Throat temperature increases with increase in injection pressure for mark1 as well as mark2 test series as shown in following figure-24. This is due to the fact that the convective heat transfer coefficient at the throat is a function of chamber pressure(Pc) raised to an exponent[20] and Pc decreases from HIP to LIP lowering the throat temperature.
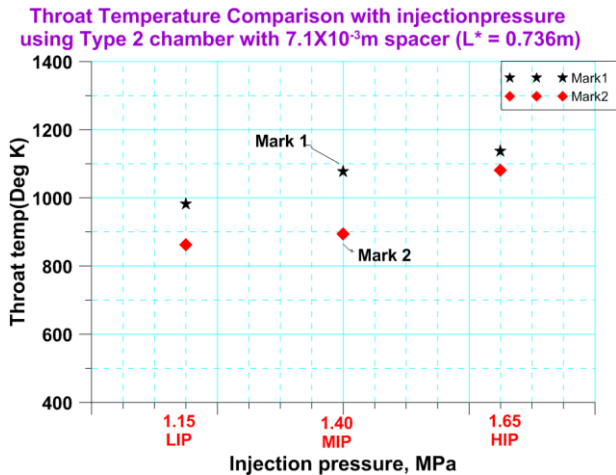

Figure-24 Mark1& Mark2 with type2 at 7.1×10^{-3}m spacer - Injection pressure on throat temp.

Throat temperature in mark2 injector test series is relatively lower in comparison with mark1 injector test series due to different spray characteristics mentioned previously.

Ignoring convergent angle variation effect as its influence on $C^*_{eff(exp)}$ is found to be marginal in the investigation, an optimum performance box with L*, L_N & CR as variables which will give a minimum $C^*_{eff(exp)}$ of 90% for the range of injection pressures evaluated is shown with green shade in the figure-25 below.
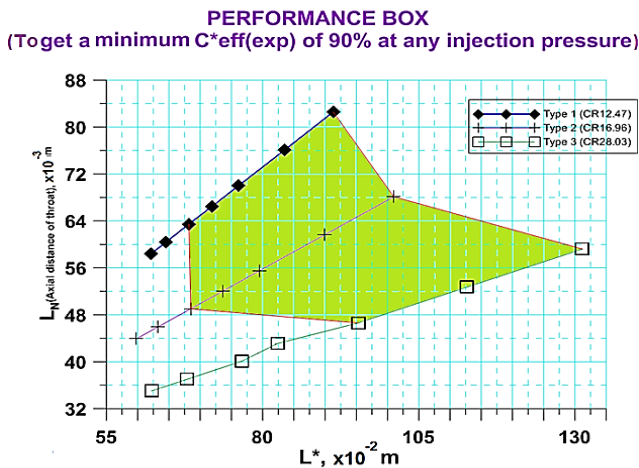

Figure-25 Optimum Performance Box

VII.   CONCLUSION

C* efficiency is influenced by propellant atomization and vaporization in the combustion chamber. Atomisation is controlled primarily by the injector design while vaporization depend upon the combustion chamber design and propellant properties. An experimental investigation is carried out to evaluate the effect of combustion chamber design parameters on performance for varied injector spray & atomisation characteristics and injection pressures. Range of injection pressures evaluated are typical of those experienced by small thrusters in its operational life in a spacecraft mission.

Two regimes of L* namely lower(L*<0.68m) and higher(L*≥0.68m) are identified where sensitivity of performance($C^*_{eff(exp)}$) and throat temperature are different. Dependence of $C^*_{eff(exp)}$ on the axial distance of the throat from the injection point of the propellant shows that the vaporization of the propellant is a dominant rate controlling process in hypergolic combustion which is the basis of the analytical model used in the investigation. Investigation also shows that $C^*_{eff(pred)}$ computed from the method of approach of using a reference/model test series closely matches with $C^*_{eff(exp)}$. However in the lower L* regimes where performance variation is highly sensitive, trend of $C^*_{eff(pred)}$ depends on the reference/model test series. CR variation study shows that thrust chamber geometry influences differently on performance at each injection pressure condition as well as regimes of L* depending on spray characteristics. Influence of convergent angle on $C^*_{eff(exp)}$ is insignificant in this study whereas it affects throat temperature with higher the angle, higher the throat temperature. Injection pressure variation study indicates that the observations seen are identical in lower L* and higher L* regimes. It can be concluded from the investigation that for a given operating conditions, there exists a range of L* and CR which will give an optimum performance in $C^*_{eff(exp)}$. Higher CR(type3, CR:28.03) limits minimum L* required to a higher value(0.953m) to get the same level of $C^*_{eff(exp)}$ of 90% in comparison with lower CR(type1, CR:12.47 gives a $C^*_{eff(exp)}$ 90% at a minimum L* of 0.682m). Due to the difference in spray characteristics, throat temperature in mark2 injector test series is relatively lower as the dry out point of film cooling will is near to the throat in comparison with mark1 injector test series. Design of combustion chamber as well as selection of spray characteristics can be finalized based on the operating temperature constraints of the material chosen.

Nomenclature

A :Cross sectional area , m²

A_s :Swirl number

CR :Contraction ratio defined as ratio of A_c/A_{thr}

C_d :Coefficient of discharge at injector exit

C^*_{eff}:C* efficiency, %

C^*_{th} :Theoretical C* at the operating conditions, m/s

d_i :Inner diameter of the inner orifice, m

d_{in} :Outer diameter of the inner orifice, m

d_o :Inner diameter of the outer orifice, m

*HIP:*High Injection pressure, MPa(Oxidiser/Fuel-1.65/1.65MPa for mark1 & 1.75/1.55MPa for mark2 version injector)

$L*$:Characteristic length of thrust chamber, m

L_c :Cylindrical length of the combustion chamber, m

L_{c90} :Length of the combustion required for the vaporization of 90% of the propellant in the combustion chamber, m

L_{ch} : Characteristic dimension of flow in the injector, m

L_{CN} :Convergent length of the thrust chamber, m

L_{ef} :Correlation parameter or effective combustion chamber length for the realised combustion chamber configuration and operating conditions, m

$L_{eff\ util}$:Effective utilization factor defined as $L_{ef} \times 100/L_{c\ 90}$,%

LIP :Low Injection Pressure, MPa(Oxidiser/Fuel 1.15/1.15MPa for mark1 & 1.25/1.05MPa for mark2 version injector)

L_N :Combustion chamber length up-to the throat, m

MIP :Medium Injection pressure, MPa(Oxidiser/Fuel-1.40/1.40MPa for mark1 & 1.50/1.30MPa for mark2 version injector)

MMD:Mass median drop size, m

MMH :Mono Methyl Hydrazine

$\dot{m}$:Mass flow rate, kg/s

MR_m :Mixture ratio ($\dot{m}_O / \dot{m}_F$) measured during test

NTO :Nitrogen Tetroxide

P_c :Chamber pressure, MPa

Re :Reynolds number of propellant in the injector

S :Nozzle shape factor defined as the ratio of Convergent Nozzle volume/($A_C * L_N$)

t_s :Propellant stay time, s

$T_{i,O,R}$:Reduced initial propellant temperature, defined as the ratio of Initial propellant temperature to Critical temperature, K

u_o :Injection velocity at injector exit evaluated from cold flow studies, m/s

V_c :Chamber Volume, m^3

v_s :Average specific volume, m^3/kg

We :Weber number of propellant

ΔP :Pressure drop of injector, MPa

Symbols

α :Included angle (half) of the spray, Degree

ρ :Density, kg/m^3

μ :Viscosity of liquid, N s/m^2

σ :Surface tension of liquid, N/m

ϕ :Coefficient of useful cross section

Suffixes

c :Combustion chamber

exp :Experiment

F :Fuel

g :Ambient gas

o :Oxidiser

pred :Predicted

p :Propellant

t :Total propellant(oxidizer and fuel together)

Thr :Throat

V :Vapour

W :Water

REFERENCE

1. Richard J.Preim and Marcus F.Heidmann, Propellant vaporization as a design criterion for Rocket Engine Combustion Chamber, Technical report R- 67.
2. Richard J.Preim and Marcus F.Heidmann, Vaporisation of Propellants in Rocket Engines, ARS 13th Annual Meeting, NewYork, November 17-21, 1958.
3. Thomas F. Seamans and Marcel Vanpee, Development of a Fundamental Model of Hypergolic Ignition in Space-Ambient Engines, AIAA Journal, pp 1616-1624, Vol.5, No.9, September 1967.
4. Timothee L. Pourpoint and William E.Anderson, Environmental Effects on Hypergolic Ignition, 41st AIAA/ASME/SAE/ASEE Joint Propulsion Conference, AIAA-2005-3581, July 10-13, 2005, Tucson, USA.
5. Swanand V. Sardeshmukh, Stephen D. Heister, Haifeng Wang, and Venkateswaran Sankaran, Kinetic Modeling of Hypergolic Propellnts, 49th AIAA/ASME/SAE/ASEE Joint Propulsion Conference, AIAA 2013-4157, July 14 - 17, 2013, San Jose, CA, USA.
6. O.Knub, D.Preclik and D.Estublier, Flow Field Prediction within Liquid Film Cooled Combustion Chambers of Storable Bi-Propellant Rocket Engines, 34th AIAA/ASME/SAE/ASEE Joint Propulsion Conference, AIAA-98-3370, 13-15 July, 1998, Cleveland, OH, USA.
7. ZHANG Lian-bo, CHU Min and XU xu, Performance Prediction of Apogee Attitude and Orbit Control Thruster for MMH/NTO Hypergolic Bipropellant, 50th AIAA/ASME/SAE/ASEE Joint Propulsion Conference, AIAA-2014-3572 July 28-30, 2014, Cleveland, OH, USA.
8. Laurent Catoire, Nabiha Chaumeix and Claude Paillard, Chemical Kinetic Model for Monomethyl hydrazine/Nitrogen Tetroxide Gas–Phase Combustion and Hypergolic Ignition, Journal of Propulsion and Power, pp 87-92, Vol.20, No.1, January-February 2004.
9. B.P.Green et al, Injection and Combustion of Hypergolic Bipropellants, Technical Report No.AFRPL-TR-69-48, April 1969.
10. D.L.Kors, L.B.Bassham and R.E.Walker, A Liquid Rocket Performance Model Based on Vaporisation Interactions, Journal of Spacecraft and Rocket, pp 1133-1138, Vol.6, No.10, October 1969.
11. Gordon Sanford and Mcbride, Computer Program for Calculation of Complex Chemical Equilibrium Composition, Rocket Performance, Incident and Reflected Shocks and Chapman-Jougnet Detonation, NASA SP 273.
12. Ulrich Gotzid and Eckhard Davies, Development Status of Astriums New 22N Bipropellant Thruster Family, 39th AIAA/ASME/SAE/ASEE Joint Propulsion Conference, AIAA-2003-4777, 20-23 July 2003, Alabama, USA.
13. A.P. Vasilyev, V.M.Kudryavstev, et al, Fundamentals of Theory and Calculation of Liquid Propellant Rocket Engines (Volume II-III), Report FTD-MT-24-253-68.
14. M.R.Soltani, K.Ghorbanian, M.Ashjaee, M.R. Morad, Spray Characteristics of a liquid – liquid coaxial swirl atomizer at different mass flow rates, Aerospace Science and Technology Journal, pp 592-604, Vol.9, Issue 7, October 2005.
15. R.C.Schindler and L.Schoenman, Development of a Five-Pound Thrust Bipropellant Engine, Journal of Spacecraft and Rockets, pp 435-442, Volume13, No.7, July 1976.
16. J.Hardgrove and H.Krieg(Jr.), High Performance Throttling and Pulsing Rocket, 20th AIAA/ASME/SAE/ASEE Joint Propulsion Conference, AIAA-84-1254, 11-13, June 1984, Ohio, USA.
17. P.Arun Kumar, C.RajeevSenan, B. Ajith et al, Investigations on the Effect of Variations in Characteristic Length(L*) and Contraction Ratio of the Combustion Chamber on the Performance of a Liquid Hypergolic Bipropellant Thruster, 65th International Astronautical Congress, paper no. IAC-14-C4.3.6, 29thSeptember-3rd October 2014, Toronto, Canada.
18. P.Arun Kumar, S.Venkateswaran, B. Ajith et al, Effect of Variation of Chamber Geometry on the Performance of a Small Scale Bipropellant Thruster, 58th International Astronautical Congress, paper no. IAC-07-C4.3.08, September2007, Hyderabad, India.
19. John R. Howell, Mary K.Strite, et al, Analysis of Heat – Transfer Effects in Rocket Nozzles Operating with very High Temperature Hydrogen, Report NASA TR- R-220.
20. George P Sutton, Oscar Biblarz, Rocket Propulsion Elements, Wiley Publications, 8th edition, January 2010.